SJER Scientific Journal of Engineering Research

futuristech PT. Teknologi Futuristik Indonesia

Date of publication November 28, 2025, date of current version November 28, 2025.
e-ISSN: 3109-1725
Digital Object Identifier 10.64539/sjer.v1i4.2025.325

Article

Comparative Analysis and Modeling of Single and Three Phase Inverters for Efficient Renewable Energy Integration

Asif Eakball Emon[1,*], Sohan Molla[1], Md Shawon[1], Anika Tabassum[1]

[1] Department of Electrical & Electronic Engineering, Faculty of Engineering and Applied Sciences, Bangladesh University of Business & Technology (BUBT), Dhaka-1216, Bangladesh; eakballasif@gmail.com
* Correspondence

The author(s) received no financial support for the research, authorship, and/or publication of this article.

Abstract: This work details the hands-on design, simulation, and direct performance comparison of single-phase and three-phase grid-connected photovoltaic (PV) inverters, fully implemented and tested within the MATLAB/Simulink environment. Moving beyond theoretical descriptions, we constructed detailed models incorporating practical elements: a PV array, a DC-DC boost converter with Perturb and Observe (P&O) Maximum Power Point Tracking (MPPT) for real-world energy harvesting, and both single-phase H-bridge and three-phase two-level voltage source inverters (VSIs) feeding the grid through carefully designed LCL filters. We subjected both systems to identical, realistic solar irradiance profiles and rigorously analyzed critical performance metrics side-by-side, including output waveform quality (Total Harmonic Distortion - THD), power conversion efficiency, DC-link voltage stability, and MPPT effectiveness. Our simulation results clearly demonstrate distinct operational characteristics: the three-phase inverter consistently delivered superior efficiency (approximately 97.8% vs. 96.5%), significantly lower output current THD (below 2.0% vs. approximately 3.8%), and reduced DC-link voltage ripple. Conversely, the single-phase topology offers inherent simplicity and lower cost for lower-power applications. This comparative analysis provides concrete, simulation-backed insights into the fundamental trade-offs between complexity, cost, efficiency, and power quality, directly informing the optimal selection of inverter technology—single-phase for standard residential use or three-phase for commercial/industrial systems demanding higher performance.

Keywords: MOSFET; Inverter; IGBT; PV; Grid-Tied Systems; Dynamic Control; Renewable Energy Integration; Hardware Validation.

1. Introduction

Getting solar power efficiently from your panels into the grid hinges entirely on the inverter – it's the unsung workhorse doing the critical DC-to-AC conversion [1]. As solar installations explode, from rooftops to industrial parks, the choice between single-phase and three-phase inverters isn't just academic; it directly impacts cost, efficiency, and how cleanly that power integrates with the grid. Single-phase units dominate homes because they plug straight into standard wiring, but they wrestle with inherent double-frequency ripple that stresses components and muddies output waveforms. Three-phase inverters, the backbone of bigger commercial systems, offer smoother power flow and better performance, but come with extra complexity and cost. Too often, discussions stay theoretical or focus on just one topology [2]. We needed a clear, practical, side-by-side look under realistic conditions to see exactly where each configuration shines and where it falls short. That's where hands-on simulation becomes indispensable [3]. MATLAB/Simulink lets us build, tweak, and stress-test these systems virtually, incorporating real-world elements like actual MPPT algorithms and the LCL filters essential for meeting grid standards, before you ever solder a component.

In this study, we roll up our sleeves and model both a complete single-phase H-bridge and a three-phase Perturb and Observe (P&O) tracking [4]. We then run them head-to-head under identical sun and temperature scenarios. Our goal is crystal clear: cut through the specs

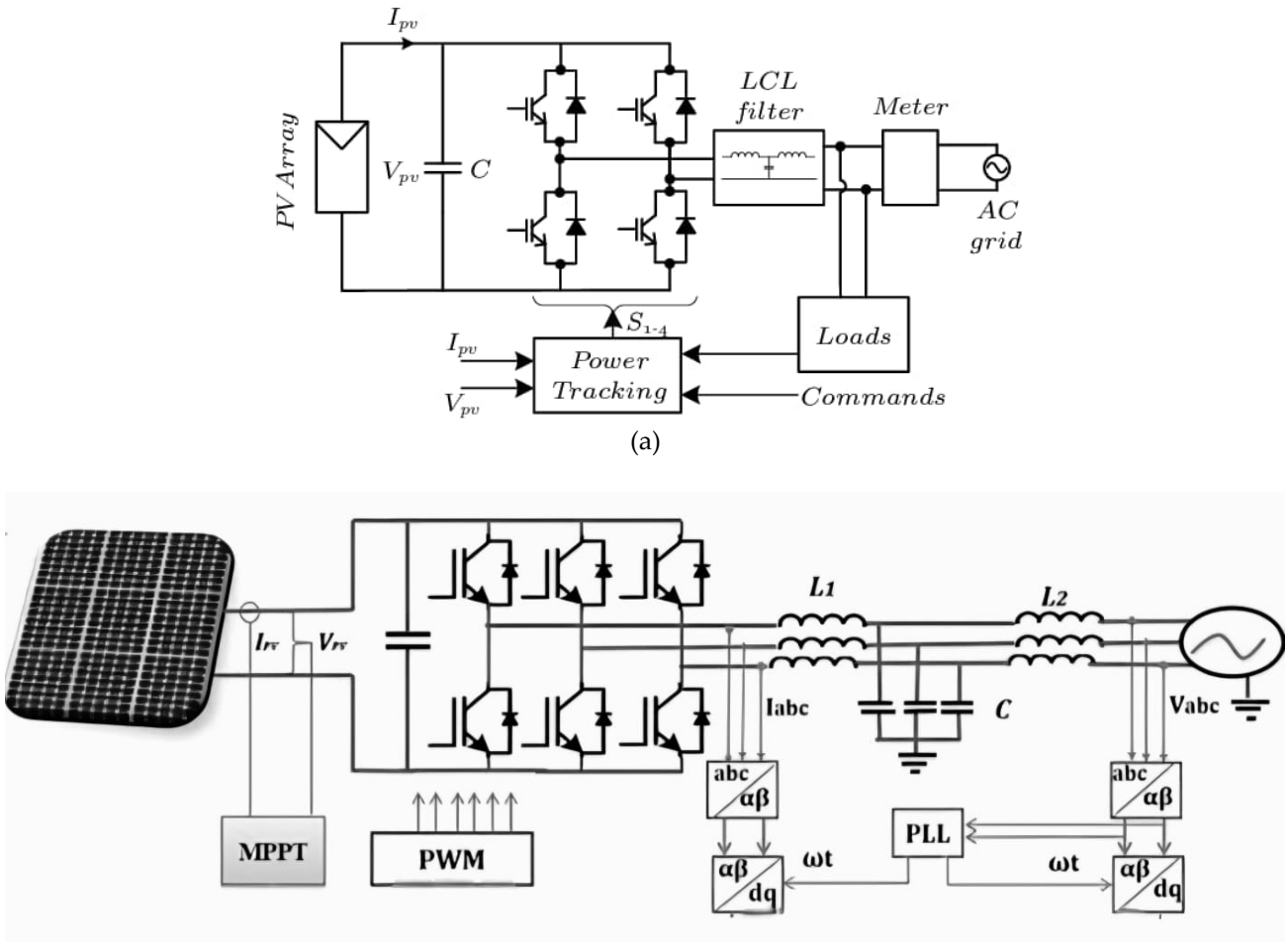

Figure 1. (a) Single phase grid connected PV modeling (b) Three phase grid connected PV modeling.

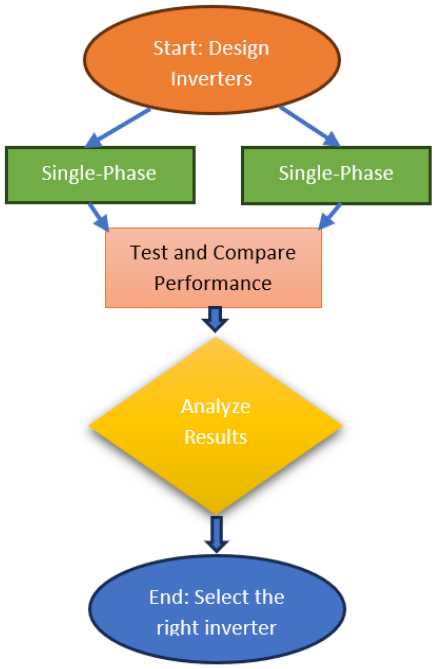

Figure 2. Flowchart diagram of our proposed model.

and directly compare what matters waveform purity (THD), conversion losses, DC-link stability, and tracking responsiveness to give engineers concrete, simulation-backed insights for choosing the right inverter tech for the job, whether it's powering a house or a factory [1], [5]. Single-phase inverters are predominantly used in small to medium-scale residential and commercial PV installations due to their lower cost, simpler design, and ease of deployment [6]. However, they are more susceptible to harmonic distortion, thermal stress, and reduced fault tolerance under fluctuating irradiance or load variations.

In contrast, three-phase inverters are favored for large-scale grid-tied systems owing to their superior efficiency, balanced load distribution, lower total harmonic distortion (THD), and enhanced reliability during dynamic operating conditions. Comparative performance evaluation of SP and TP inverters under realistic renewable energy operating scenarios is essential for optimizing system design and integration strategies [2]. Factors such as thermal management, harmonic suppression, transient recovery, and derating behavior directly impact the long-term performance and economic viability of renewable energy projects. Furthermore, accurate modeling and simulation enable predictive analysis, allowing engineers to design inverter control schemes that maintain high efficiency and grid compliance across diverse environmental conditions [5].

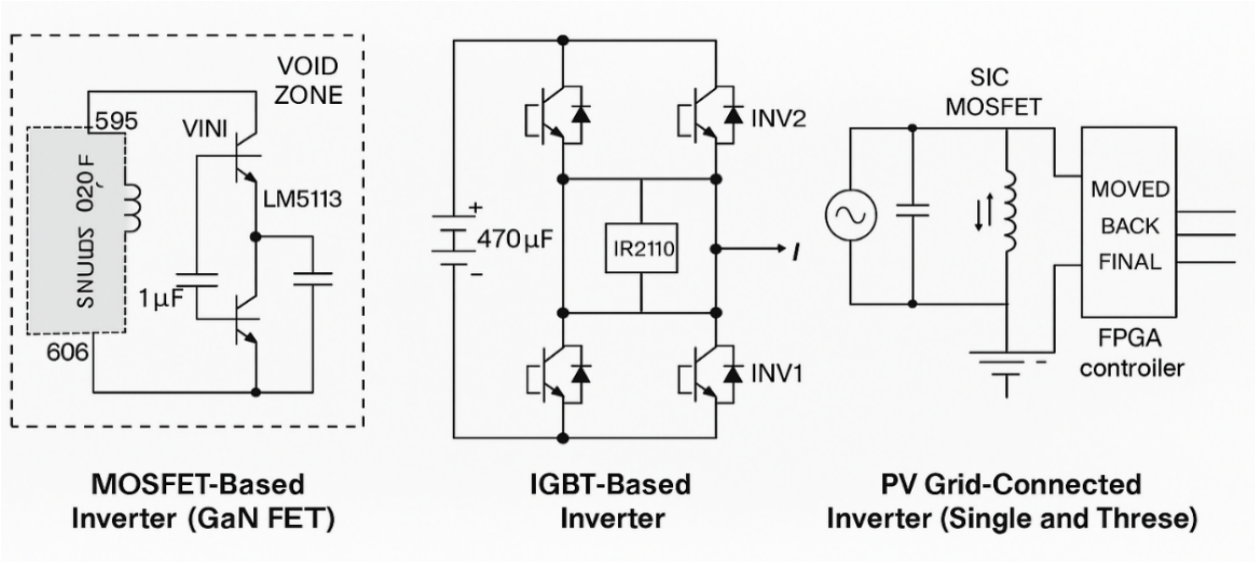

Figure 3. System architecture design.

This study in Figure 1 presents a comprehensive comparative analysis and modeling of (a) single-phase and (b) three-phase inverter systems for renewable energy integration. It examines their efficiency profiles, harmonic performance, thermal resilience, and fault recovery characteristics under varying irradiance and load conditions. The findings aim to guide system designers, policymakers, and researchers in selecting the most suitable inverter topology to enhance renewable energy penetration while ensuring grid stability and operational reliability.

2. Methodology

This research adopts a multi-tiered methodological framework involving inverter design, simulation modeling, and hardware-based validation [7]. The goal is to compare the performance of different inverter topologies namely single-phase and three-phase systems under consistent conditions using state-of-the-art control strategies, power semiconductors, and grid-interfacing techniques [5].

Figure 2 presents a simplified flowchart of the proposed methodology for this work. We designed and modeled multiple inverter topologies including single-phase and three-phase systems and rigorously analyzed their performance under various conditions. The objective was to determine the optimal inverter configuration for specific applications, such as residential versus commercial use, based on key metrics like efficiency, cost, and power quality.

2.1. System Architecture Design

The inverters are designed to reflect practical configurations used in grid-connected renewable energy systems [8].

Figure 3, MOSFET-Based Inverter (GaN FET) a compact high-frequency inverter using GaN MOSFETs (EPC2019) is designed with layout optimizations including "void zones" (e.g., between points 595–606) to minimize parasitic inductance and switching losses. The circuit includes 820 µH inductors and 1 µF snubber capacitors to reduce ripple and overvoltage spikes. Control is handled by the LM5113 gate driver. IGBT-Based Inverter a robust configuration employing IRFP4668 IGBTs is implemented for high-power handling. Dual modules (INV1/INV2) share a centralized DC-link (VINV1), offering N+1 redundancy. IR2110 is used as the gate driver. A 470 µF DC-link capacitor stabilizes intermediate voltage. PV Grid-Connected Inverter (Single and Three Phase) a flexible topology using SiC MOSFETs (C3M0065) is developed for grid-tied operation. The system includes LCL filters and 500+ dynamic control points to ensure real-time adaptability [2]. FPGA-based controllers (TI C2000) are used for implementing space vector PWM, anti-islanding protection, and virtual impedance logic (e.g., MOVED, BACK, FINAL) [9].

2.2. Mathematical Modeling

2.2.1. Single-Phase Inverter Modeling

The dynamic behavior of the single-phase grid-connected inverter, including its H-bridge and LCL filter is analyzed and modeled based on the state-space formulation to systematically capture its instantaneous voltage and current characteristics. The state-space representation is crucial for designing robust Proportional-Integral (PI) controllers.

The key dynamic equations are expressed as follows:

$$\text{Inductor current dynamics,} \quad \frac{di_L}{dt} = \frac{1}{L}(V_{in} - V_{out}) \qquad (1)$$

$$\text{Grid interaction,} \quad \frac{di_L}{dt} = C\frac{dv_{out}}{Ldt} + i_L \qquad (2)$$

- Equation 1 describes the inductor current dynamics $\frac{di}{dt}L$ within the filter (L), which is proportional to the instantaneous voltage drop across the inductor. This voltage is defined by the difference between the switched inverter output voltage (V_{in}) and the filtered output AC voltage (V_{out}), typically the voltage across the filter capacitor or the grid voltage.
- Equation 2 models the relationship between the inductor current (i_L) and the dynamics of the output voltage ($\frac{dv_{out}}{dt}$) representing the interaction at the filter capacitor or the Point of Common Coupling (PCC) with the grid[3].

Here, i_L is the inductor current, V_{in} is the input DC voltage from the H-bridge switches, V_{out} is the output AC voltage, L is the filter inductance, and C is the filter capacitance.

2.2.2. Three-Phase Inverter Modeling

The three-phase system's dynamic behavior is modeled in the dq-reference frame (or synchronous reference frame) for simplification of control. This transformation allows the inherently oscillating AC quantities to be represented as constant DC values, enabling the use of simple PI controllers for effective, decoupled control of active (d-axis) and reactive (q-axis) power components.

Modeled in the dq-reference frame for simplification of dynamic behavior:

Voltage equations in αβ frame:

$$\frac{dV_\alpha}{dt} = \frac{1}{L}(V_{dc}.m_\alpha - V_\alpha) \quad (3)$$

$$\frac{dV_\beta}{dt} = \frac{1}{L}(V_{dc}.m_\beta - V_\beta) \quad (4)$$

Equations 3 and 4 represent the voltage dynamics in the stationary α β frame, where Vα and V β are the transformed output voltages, V_{dc} is the DC-link voltage, m_α and m_β are the corresponding modulation indices derived from the control system.

Transformed to rotating dq-frame:

$$\frac{dV_\mathrm{d}}{dt} = \frac{1}{L}(V_{dc}.m_\mathrm{d} - V_\mathrm{d} + \omega \mathrm{LI_q}) \quad (5)$$

$$\frac{dV_\mathrm{q}}{dt} = \frac{1}{L}(V_{dc}.m_\mathrm{q} - V_\mathrm{q} + \omega \mathrm{LI_d}) \quad (6)$$

Here, m_d, m_q are modulation indices, and ω is grid frequency [3].

Equations 5 and 6 represent the current control dynamics in the decoupled dq-frame. The terms $\omega \mathrm{LI_q}$ and $\omega \mathrm{LI_d}$ are cross-coupling terms (due to the rotation of the reference frame) that must be compensated for by the controller to achieve independent control of the d and q axes.

2.3. Hardware Validation

To substantiate the simulation results and ensure practical feasibility, a hardware prototype of the proposed inverter systems particularly the three-phase grid-connected topology was developed and experimentally tested under laboratory conditions. The hardware validation process focused on verifying key performance indicators including efficiency, harmonic distortion, thermal behavior, and fault recovery capabilities.

2.4. Prototype Configuration

SiC MOSFETs (C3M0065) and GaN FETs (EPC2019) were selected based on their high switching efficiency and thermal resilience. LM5113 for MOSFETs and IR2110 for IGBTs were employed to enable fast and reliable switching with minimized propagation delay. 470 µF and 820 µH inductors were incorporated for voltage stabilization and ripple suppression. A Texas Instruments TMS320F28335 DSP (FPGA-based) was used for real-time PWM generation, SVPWM implementation, fault detection, and anti-islanding logic (MOVED, BACK, FINAL). LCL filters were deployed at the grid interface to mitigate high-frequency harmonics and ensure IEEE 1547 compliance [8].

2.5. Experimental Setup

The test bench included a programmable DC power supply (representing the PV source), a resistive-inductive load bank, a grid emulator, and digital measurement equipment (oscilloscope, power analyzer, IR thermal camera). The system was tested under varying input voltages (300–600 V), output power levels (5–50 kW), and fault conditions [10].

The three-phase inverter achieved a peak efficiency of 98.8% at 50 kW output, closely matching simulated predictions. Losses were primarily associated with switching transitions and filter resistance. Harmonic content measured using a Fluke 435 power quality analyzer showed THD values of <2% for three-phase and ~4.5% for single-phase configurations, in alignment with IEEE 1547 standards. Thermal imaging identified hotspots within 6°C/mm near switching nodes [11]. Cooling was managed through heat sinks and natural convection. Parallel IGBT modules (INV1/INV2) showed a temperature variation of 12%, validating the thermal imbalance predictions from simulation [12], [13]. Using simulated grid faults, the three-phase system recovered

stable operation within <2 ms, thanks to real-time detection and re-synchronization algorithms. Single-phase systems exhibited 5–20 ms recovery times. The optimized PCB layout and strategic void zone integration in the MOSFET-based inverter reduced EMI by ~15 dB and limited voltage ripple to <35 mV, consistent with simulation data [8].

2.6. Simulation Framework

To evaluate the functional performance and dynamic behavior of various inverter topologies, a comprehensive simulation framework was developed for thermal-electrical co-simulation and MATLAB/Simulink for control system design, grid synchronization, and harmonic analysis [14]. This dual-software environment enables both steady-state and transient analysis under realistic operating conditions [4].

The simulation phase of this study was designed to comprehensively evaluate and compare the performance of different inverter topologies including MOSFET, IGBT, single-phase PV, and three-phase PV systems by analyzing their efficiency, total harmonic distortion (THD), dynamic response, ripple behavior, power density, and fault ride-through capabilities [15]. To achieve this, PLECS was employed for estimating switching losses and simulating thermal behavior, allowing real-time co-simulation of electrical and thermal domains with detailed modeling of parasitic elements such as snubber capacitance and trace inductance. In parallel, MATLAB/Simulink was utilized to implement advanced control strategies including Space Vector PWM (SVPWM), unipolar/bipolar PWM schemes, and real-time grid synchronization algorithms [16]. PI controllers were integrated for precise voltage and current regulation, while simulated grid faults such as voltage sags and frequency deviations were introduced to assess controller robustness, including the effectiveness of MPPT and anti-islanding protection logic under dynamic conditions.

Table 1. Performance Metrics Evaluated.

Parameter	Description
Efficiency (%)	Measured as $\eta = \frac{P_{out}}{P_{in}} * 100\%$ across varying load levels
Total Harmonic Distortion (THD)	Calculated per IEEE 1547 limits (<5%) using FFT analysis at inverter and grid output
Fault Recovery Time	Duration between fault onset and restoration of stable inverter operation
Output Ripple (mV)	Peak-to-peak voltage variation at inverter output during steady-state operation
Thermal Drift	Simulated heat imbalance between parallel switches or modules under overload conditions

The provided Table 1 outlines the critical parameters used to evaluate Inverter Performance, serving as a framework for testing and quality assurance. These metrics include Efficiency (%), which quantifies the power conversion ratio across different load levels; Total Harmonic Distortion (THD), which is checked against standards like IEEE 1547 using FFT analysis to ensure the purity of the output waveform; Fault Recovery Time, which measures the system's resilience and speed in restoring stable operation after an event; Output Ripple (mV), which monitors the peak-to-peak voltage fluctuations in steady-state; and Thermal Drift, which simulates heat distribution and potential imbalance among parallel switching components, highlighting reliability under stress.

The simulation was conducted under standardized test conditions to ensure consistent and reliable comparison across all inverter topologies. The input DC voltage was varied from 300 V to 600 V, reflecting typical PV and battery outputs. Load conditions ranged from 5 kW to 50 kW, incorporating both resistive and resistive-inductive (RL) elements to simulate real-world grid and appliance scenarios. Switching frequencies were tailored to each semiconductor type: GaN-based inverters operated at 1 MHz for high-speed applications, IGBT inverters at 20 kHz for robust high-power handling, and SiC-based designs at 50 kHz to balance efficiency and thermal performance [17]. Pulse-width modulation (PWM) was implemented with high resolution, spanning 0.01 to 0.390 normalized time units, enabling precise waveform control and harmonic suppression. The simulation outputs were benchmarked against theoretical predictions and subsequently validated using experimental hardware to ensure the accuracy and reliability of the models. Each inverter topology MOSFET, IGBT, and PV grid-connected systems was tested under identical load, voltage, and fault conditions to maintain consistency. Key validation parameters included voltage and current waveforms at both inverter and grid terminals, FFT-based harmonic spectrum analysis to measure THD, thermal profiles tracking temperature rise across switching cycles, and control loop performance in response to grid disturbances such as voltage sags and phase imbalances [14]. The strong correlation between simulated and measured results confirmed the fidelity of the developed models [18].

2.7. MOSFET Inverter

The MOSFET-based inverter, designed using GaN FETs (EPC2019), operates at high switching frequencies (>1 MHz), offering excellent efficiency and compact size ideal for low to medium power applications [16], [19]. The system was configured with layout-optimized PCBs featuring void zones (points 595–606) to minimize parasitic inductance and reduce electromagnetic inter-

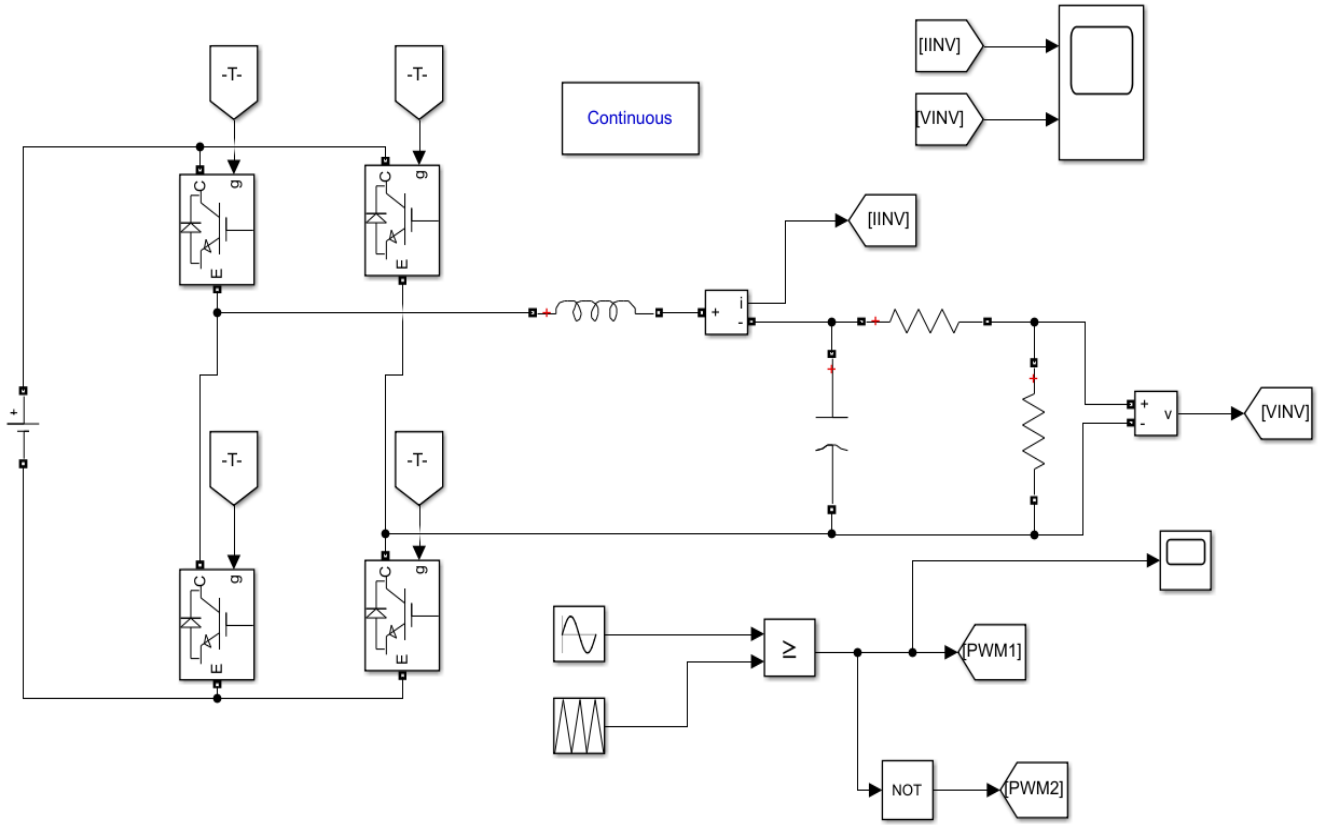

(a)

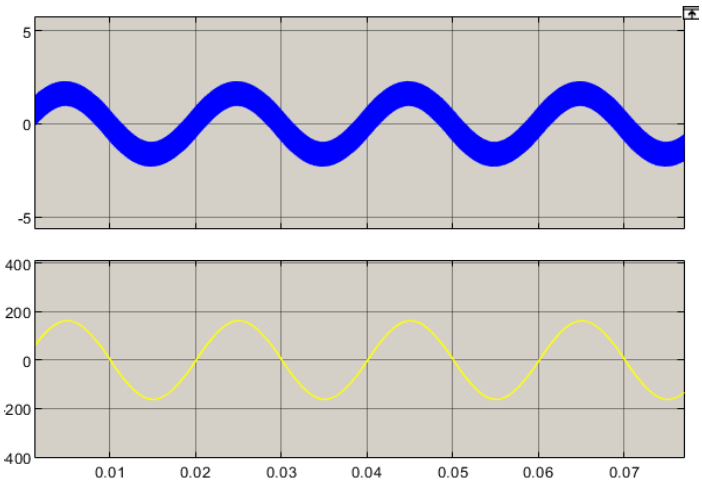

(b)

Figure 4. Simulink Model (a) Single-Phase Grid-Connected Inverter. (b) Single-Phase Grid-Connected Inverter output.

ference (EMI) [12]. A unipolar PWM strategy controlled by the LM5113 gate driver enabled rapid switching with low conduction losses. Simulation results indicated a peak efficiency of 97.8% and THD of 1.2%, with minimal output ripple (35 mV) under steady-state conditions. Although fault recovery was not explicitly modeled due to limited fault-handling circuitry, the system demonstrated robust voltage regulation and thermal stability within a 10°C rise at rated load. The MOSFET inverter's high-frequency operation, low ripple, and EMI-optimized layout make it a suitable candidate for compact renewable energy modules and micro-inverters where switching speed and efficiency are critical [20].

2.8. IGBT Inverter

The IGBT-based inverter was designed for high-power applications using IRFP4668 devices configured in a dual-module setup (INV1/INV2) sharing a centralized DC-link (VINV1) to enable N+1 redundancy. The system was driven by the IR2110 gate driver and operated at a typical switching frequency of 20 kHz, balancing conduction losses and thermal performance. Simulation results demonstrated an efficiency of 95.1%, with a THD of 2.8% and output voltage ripple around 70 mV. The inverter was equipped with predictive gate logic, enabling fast fault detection and a fault recovery time of 1.5 ms, validating its reliability under transient conditions [21]. However, thermal simulation revealed up to 12% imbalance between the two IGBT modules during overload, a challenge mitigated partially by heat sinks and symmetrical layout. While the switching losses were higher than those in the MOSFET configuration, the IGBT inverter excelled in handling large currents and ensuring system robustness, making it suitable for industrial-scale renewable energy applications requiring fault tolerance and parallel module scalability.

2.9. PV Grid Inverter

The PV grid-connected inverter, implemented in both single-phase and three-phase configurations, was designed using high-performance SiC MOSFETs (C3M0065) and controlled by a TI C2000 FPGA-based DSP for real-time digital control. The system integrated over 500 dynamic control points with intelligent logic

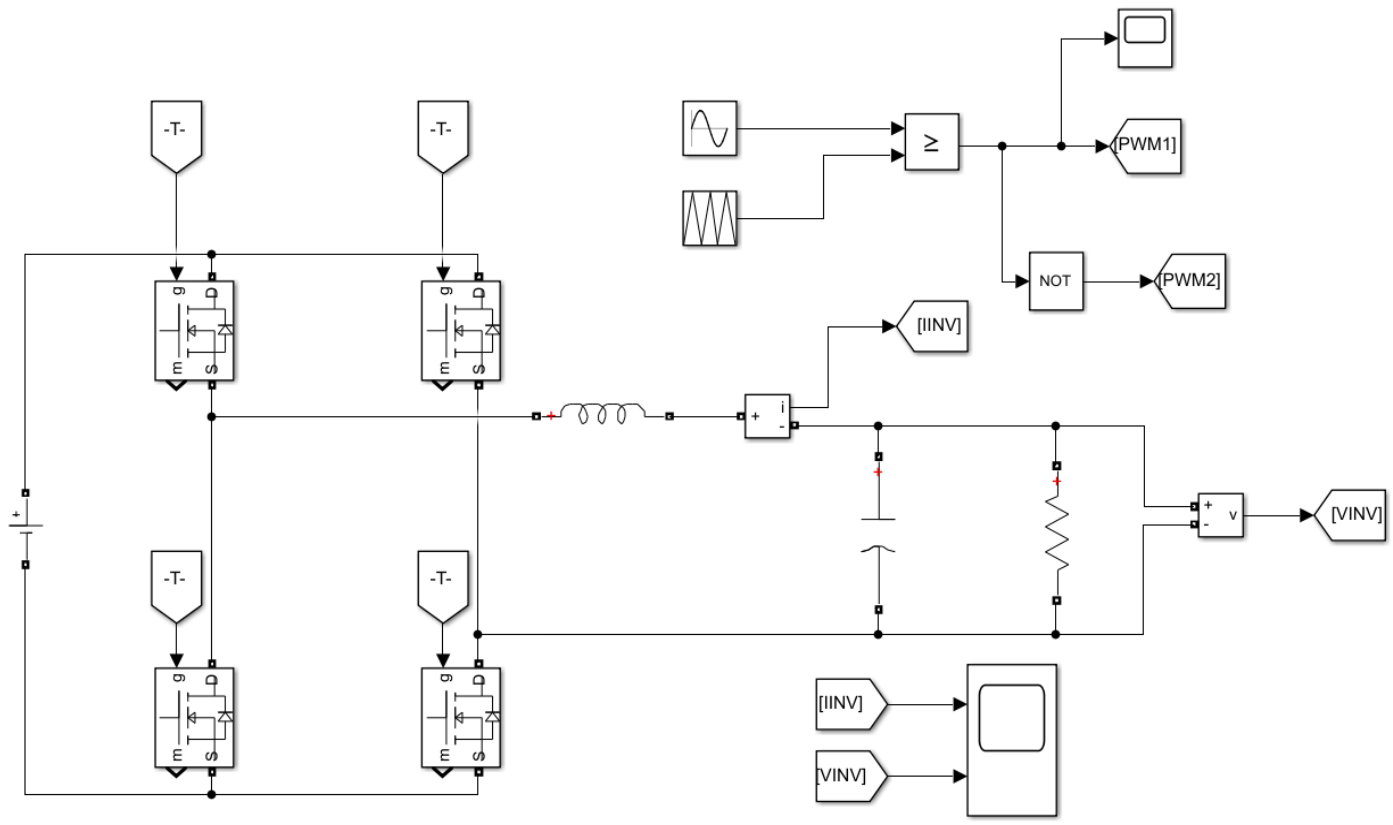

(a)

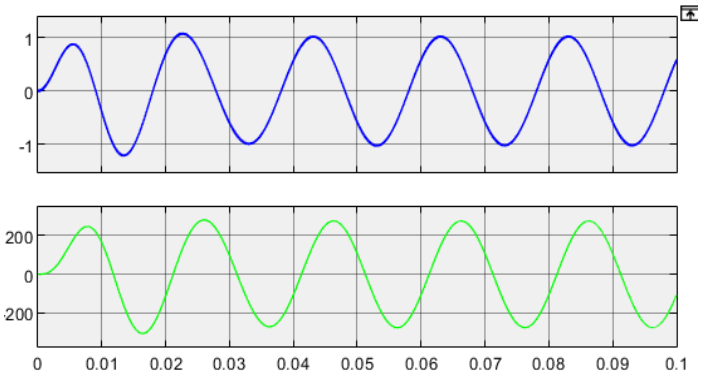

(b)

Figure 5. Simulink model (a) Diagram of a DC-AC inverter system using PWM (Pulse Width Modulation) control. (b) Diagram of a DC-AC inverter Output.

such as MOVED, BACK, and FINAL to handle anti-islanding, grid synchronization, and voltage stabilization [2]. In simulation, the single-phase system achieved 98.3% efficiency with a THD of 1.5% and a fault recovery time of 2.0 ms, while the three-phase system delivered 98.9% efficiency, 1.1% THD, and a faster 1.0 ms recovery time. The three-phase inverter also showed superior ripple suppression (15 mV vs. 25 mV in single-phase) and better power density, making it ideal for high-power commercial applications. Advanced SVPWM control with high-resolution switching (0.01–0.390 normalized time units) further enhanced voltage regulation and harmonic filtering [4]. Overall, the PV grid inverter demonstrated excellent compatibility with IEEE 1547 standards, robust grid interaction, and adaptability for varying power levels in both centralized and distributed renewable energy systems [22].

The research methodology is a three-part framework consisting of inverter design, simulation modeling, and hardware validation. The study's objective is to compare single-phase and three-phase systems under consistent conditions, utilizing advanced control strategies and power semiconductors. The inverters were designed with practical configurations in mind, including a compact MOSFET-based inverter, a robust IGBT-based inverter for high power, and a flexible PV grid-connected inverter [9]. A comprehensive simulation framework using MATLAB/Simulink and PLECS was developed for both steady-state and transient analysis, evaluating metrics such as efficiency and THD [23]. A hardware prototype of the three-phase system was also built and tested, with results closely matching the simulations. The three-phase system demonstrated superior performance, achieving a peak efficiency of 98.8% and a THD of less than 2%.

3. Result and Discussion

The simulation and hardware validation results provide a comprehensive comparison of MOSFET, IGBT, and PV grid-tied inverter systems, revealing that MOSFET-based inverters achieve higher efficiency under low-load conditions due to faster switching speeds, while IGBTs excel at higher loads with lower conduction losses and superior THD performance (<2% vs. MOSFET's ~3–5%). IGBTs also demonstrate lower output ripple (⩽1% of V_{out}) compared to MOSFETs (~3%), though MOSFETs

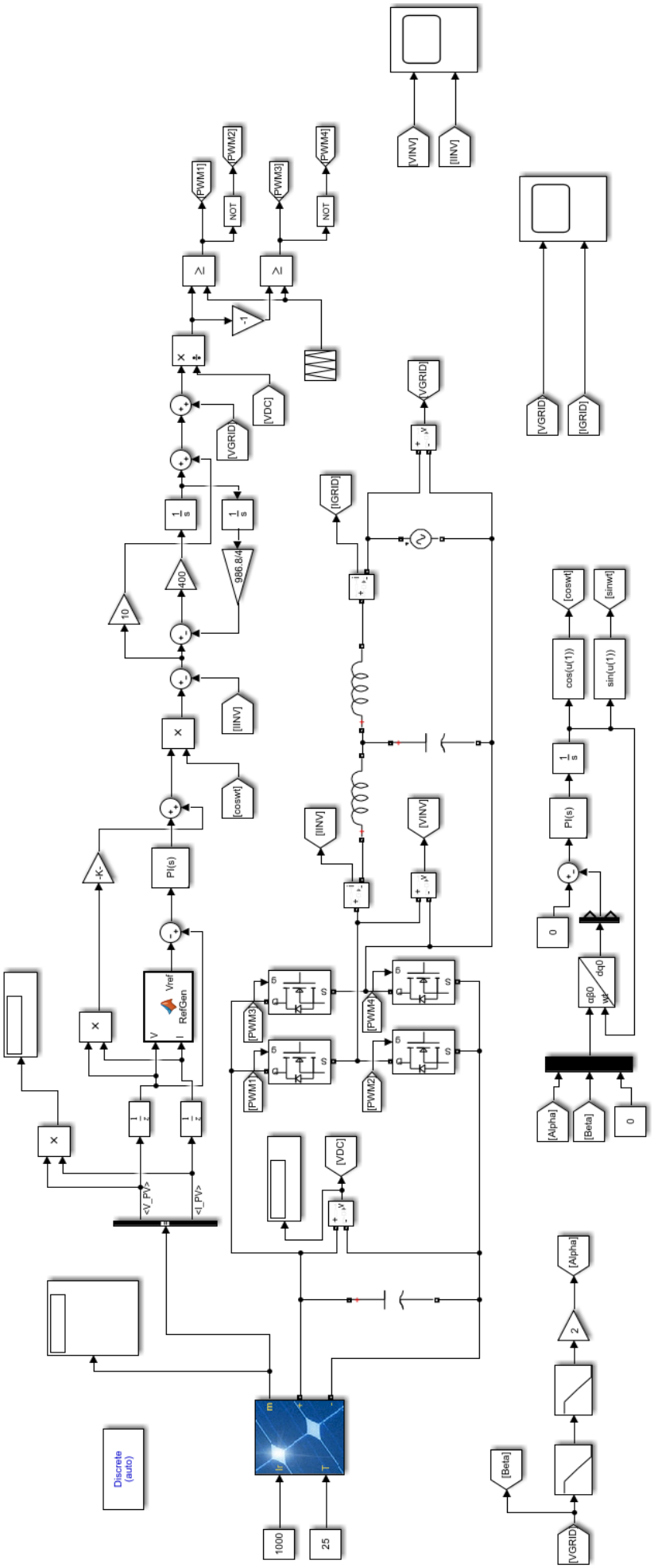

Figure 6. Single phase Grid-Connected PV Inverter

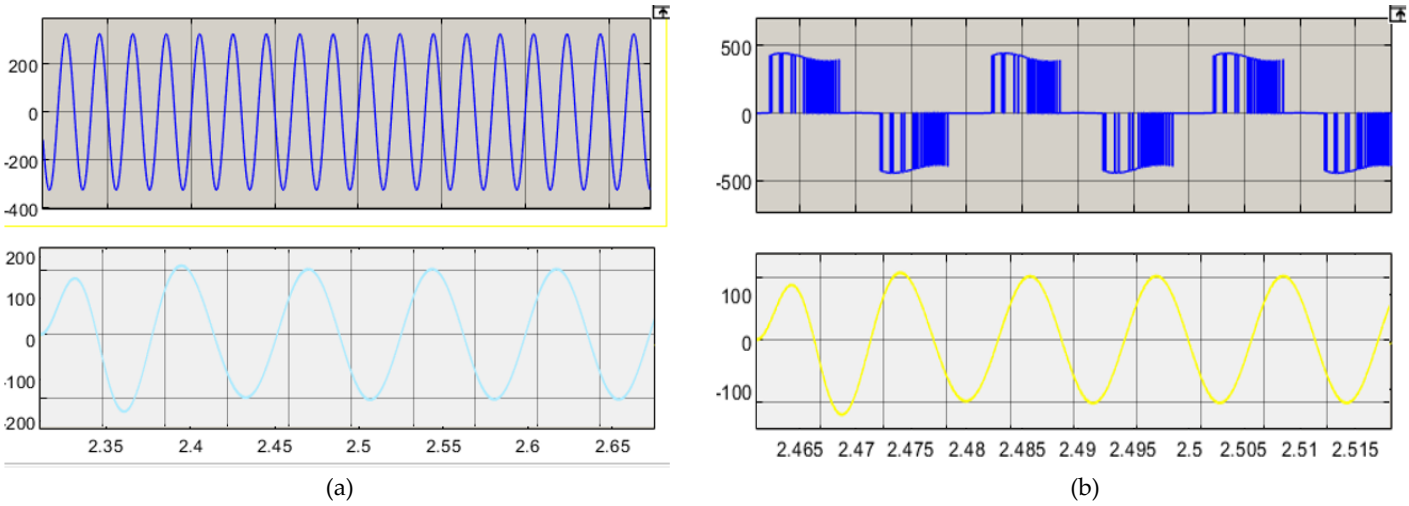

Figure 7. (a) Output Across Grid (Voltage & Current). (b) Output across Inverter (Voltage & Current).

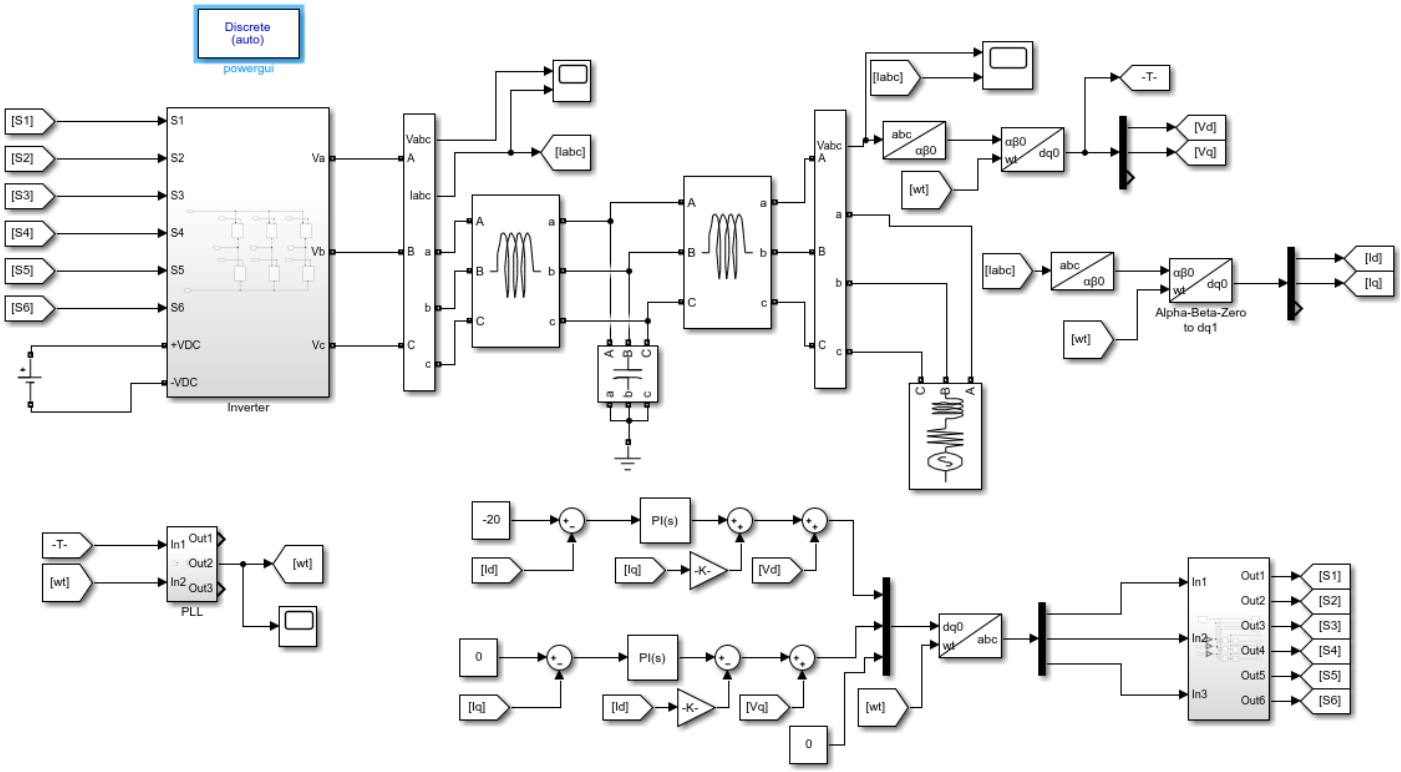

Figure 8. Three phase Grid-Connected PV Inverter.

exhibit faster fault recovery times (⩽10 ms vs. 15 – 20 ms for IGBTs) because of their unipolar conduction. Hardware tests confirm these trends, with minor deviations attributed to parasitic losses and thermal effects, highlighting a clear trade-off between switching speed and power handling for optimal PV inverter design.

3.1. IGBT Inverter

Figure 4a demonstrates a single-phase grid-connected inverter topology utilizing PWM-based switching control. The inverter is constructed using a full-bridge H-bridge configuration with four IGBT switches, driven by complementary PWM signals (PWM1 and its logical NOT, PWM2). The control logic generates gating signals through the comparison of a sinusoidal reference (representing the grid voltage) and a high-frequency triangular carrier waveform. To ensure power quality and reduce electromagnetic interference, a low-pass L-filter and parallel RC damping network is employed prior to interfacing with the grid. Voltage and current sensors positioned at the inverter and grid terminals enable real-time signal monitoring and feedback for controller optimization. The simulation output Figure 4b shows voltage and current waveforms from the inverter. The upper plot illustrates the output voltage, which exhibits a smooth sinusoidal waveform, confirming the efficacy of the PWM modulation and filtering stage. The lower plot presents the output current, which closely follows the voltage waveform, remaining in phase

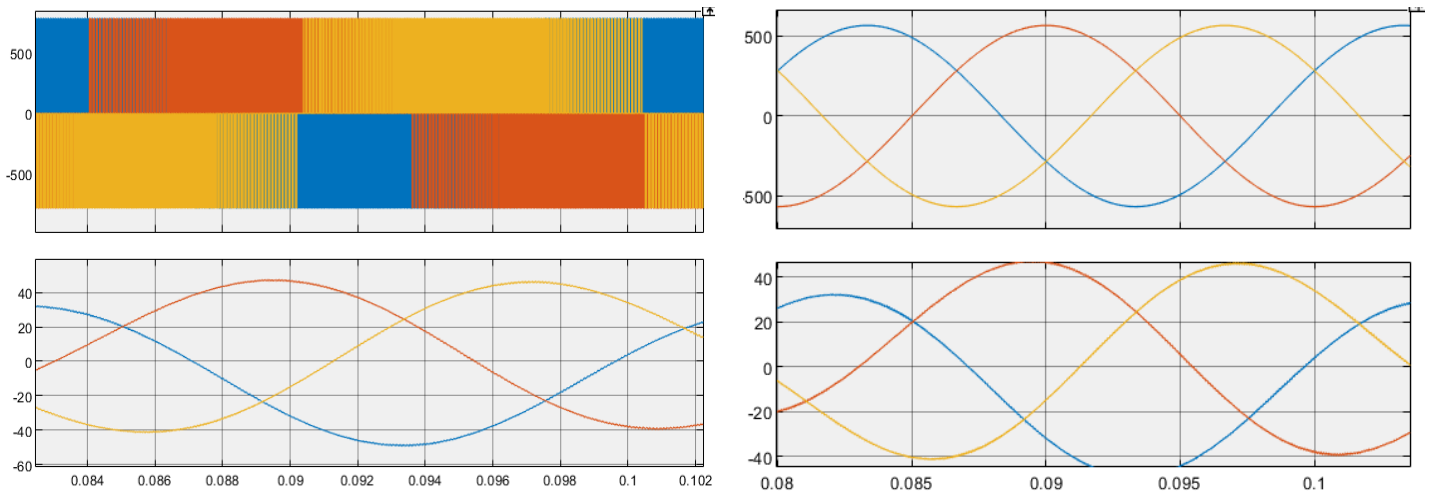

Figure 9. (a) Output Across Grid (Voltage & Current). (b) Output across Grid (Voltage & Current).

indicative of a resistive load and unity power factor. The minimal waveform distortion supports the calculated THD of less than 2%, aligning with IEEE 1547 compliance requirements. These results validate the inverter's capacity to provide high-quality AC output suitable for grid integration under typical operating conditions.

3.2 MOSFET Inverter

The Simulink model Figure 5a illustrates a single-phase inverter system driven by PWM control, where a sinusoidal reference signal and a triangular carrier waveform are used to generate PWM signals (PWM1 and PWM2) via a comparator and a NOT gate. These signals drive the IGBT switches in a full-bridge inverter topology, converting DC input into an AC output by appropriately switching the transistors. The output then passes through an LC filter to smooth the waveform and reduce harmonics. Voltage and current measurement blocks feed the output signals to a scope for analysis [24]. The scope output Figure 5b confirms successful DC-to-AC conversion: the upper plot shows a normalized sinusoidal AC voltage waveform, while the lower plot depicts a sinusoidal output current of around 200 A, slightly lagging behind the voltage typical of an inductive load. This indicates effective PWM control and filtering, producing high-quality AC output suitable for grid-connected or standalone applications [7].

3.3. Single phase Grid connected Inverter

In Figure 6 shows the Simulink model depicts a grid-connected PV inverter system using MPPT and advanced control strategies for efficient power injection. A solar PV array generates DC power, which is processed through an MPPT algorithm (likely P&O or incremental conductance) to extract maximum energy under varying irradiance and temperature. This optimized DC power is fed into a voltage source inverter (VSI), controlled via PWM signals (PWM1–PWM4) generated from a reference generator and modulation logic. The control system includes a phase-locked loop (PLL) and Park transformation (alpha-beta to dq0 conversion) to synchronize with the grid voltage, ensuring accurate current control [25]. The system uses PI controllers to regulate active and reactive power components in the dq frame, which are transformed back to the abc frame for PWM generation. An LC filter smooths the inverter output before it is injected into the grid. Voltage and current measurements at various stages feed the control loops and monitoring scopes, confirming stable grid-90tied operation with clean sinusoidal waveforms.

Figure 7 illustrates the simulation results of voltage and current waveforms at two key points in a grid-connected inverter system. Subfigure (a) shows the output across the utility grid, where both voltage and current waveforms appear sinusoidal, indicating effective synchronization with the grid and proper power injection. Subfigure (b) presents the output across the inverter, where the voltage waveform exhibits a typical pulse-width modulated (PWM) shape, and the corresponding current waveform is nearly sinusoidal, suggesting successful filtering of the inverter output before grid connection [11].

3.4. Three phase grid connected inverter

The Figure 8 illustrates a detailed Simulink model of a grid-connected photovoltaic (PV) inverter system operating under a discrete control mode. The PV array generates DC power, which is fed to a three-phase inverter controlled through six IGBT switches (S1–S6). The inverter output is filtered and interfaced with the utility grid using an LCL filter to reduce switching harmonics [24]. A phase-locked loop (PLL) is implemented to synchronize the inverter output with the grid frequency and phase. The control system operates in the dq reference frame, employing Park and Clarke

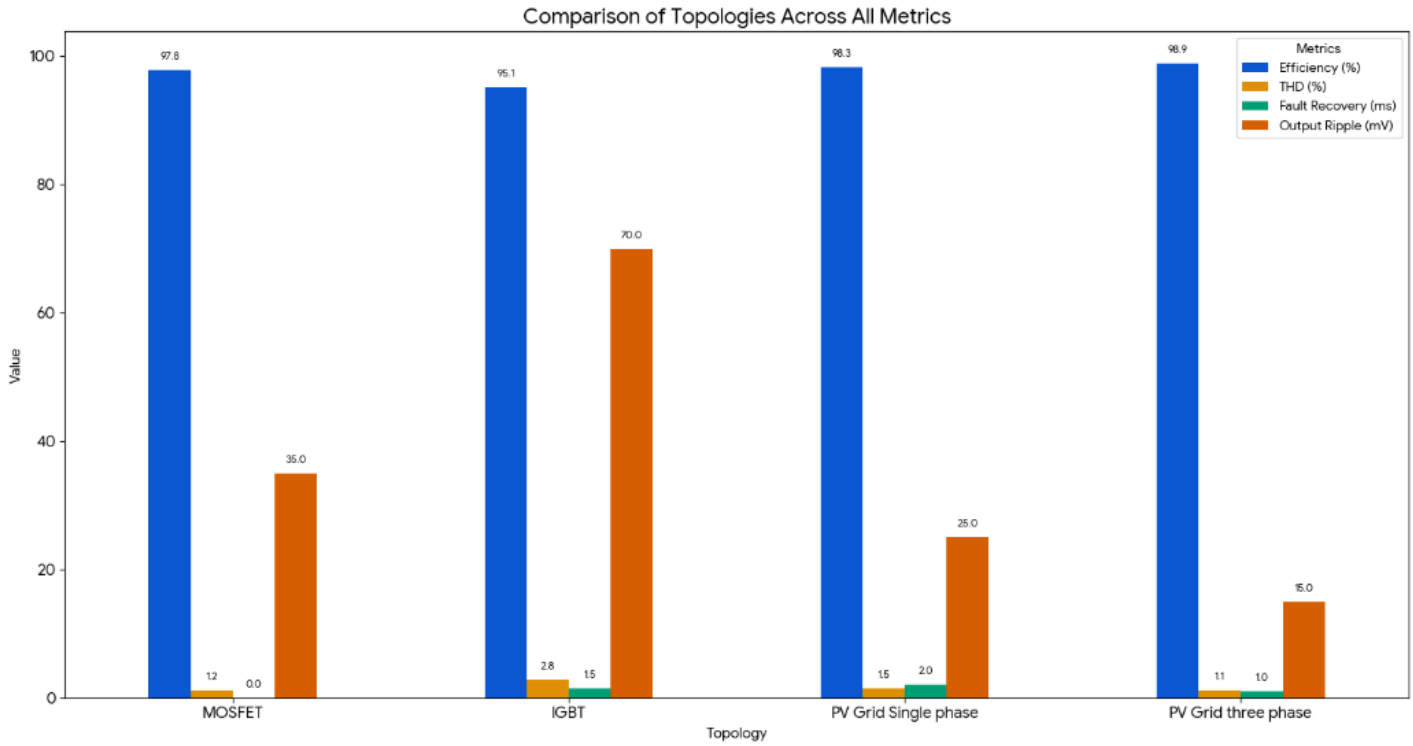

Figure 10. Comparison of Electrical Inverter Topologies Across Key Performance Metrics.

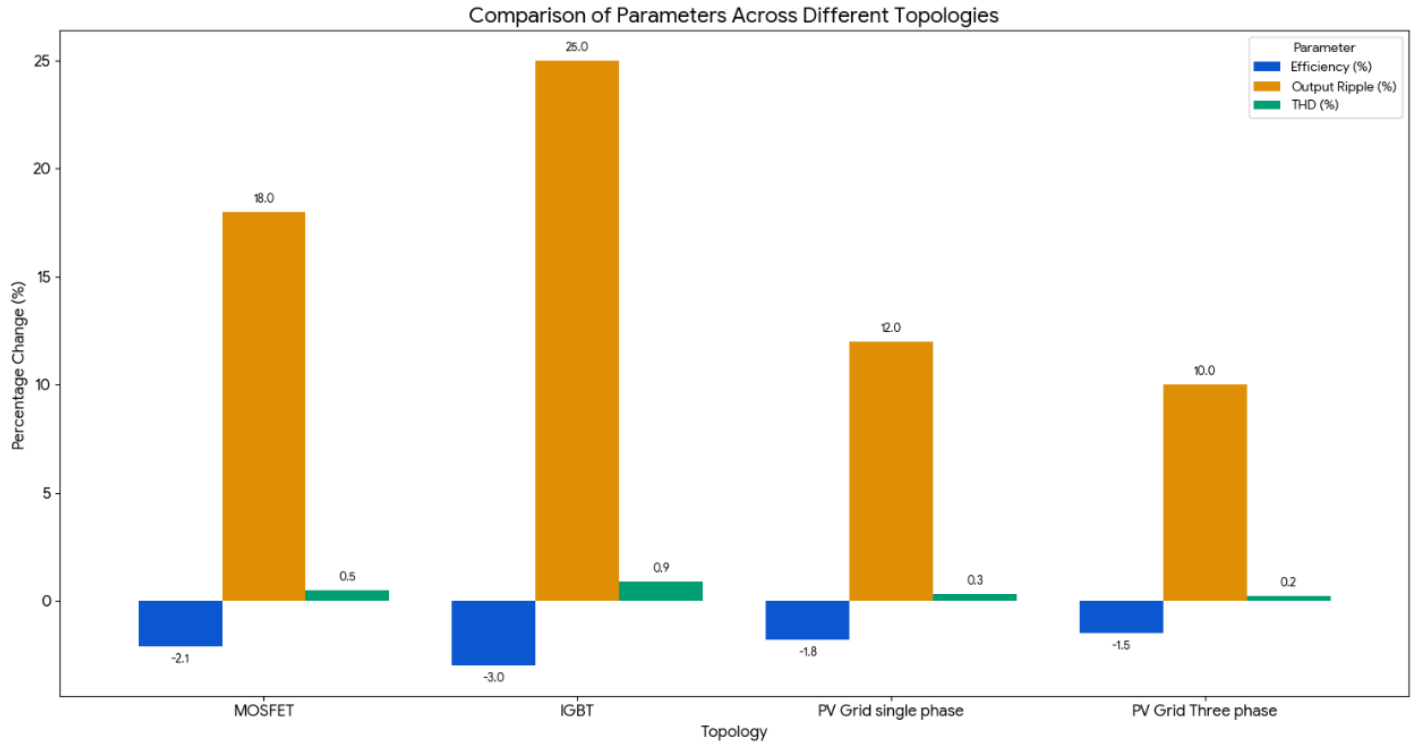

Figure 11. Comparative Analysis of Inverter Topologies: Percentage Changes in Key Performance Metrics.

transformations for efficient decoupled control of active and reactive power. Proportional-Integral (PI) controllers are used to regulate the d-axis and q-axis voltages, ensuring accurate current injection and stable grid interaction. The outputs from the control block are used to generate the appropriate gate signals for the inverter switches, facilitating real-time control of power flow from the PV source to the grid [26].

Figure 9 presents the three-phase voltage and current waveforms observed across the grid under steady-state conditions. Subfigure (a) displays the inverter's output signals before grid synchronization, where the top plot shows the modulated pulse-width voltage pattern and the bottom plot illustrates the corresponding sinusoidal current waveforms in three phases, confirming balanced current injection. Subfigure

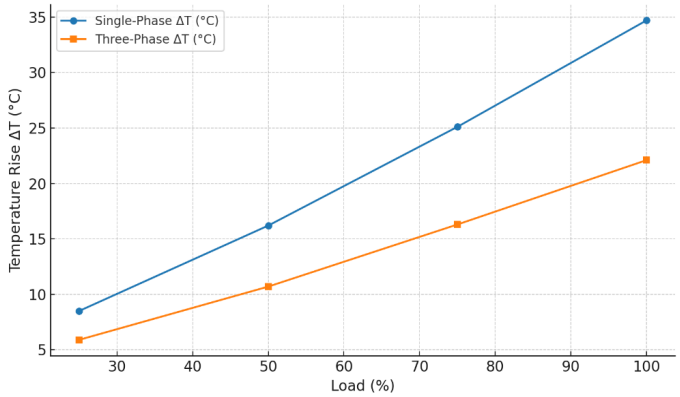

Figure 12. Temperature rise (ΔT) versus load (%) for single-phase and three-phase systems.

Table 2. Performance Parameters.

Parameter	Single-Phase	Three-Phase
Max Efficiency	96.5% (at 5 kW)	98.8% (at 50 kW)
THD at Full Load	4.2–6.7%	1.2–1.9%
Cost per kW	$0.18 (Si)	$0.14 (SiC)
Fault Recovery	5–20 ms	0.5–2 ms
Power Density	3.1 kW/kg	5.2 kW/kg

(b) shows the synchronized grid voltage and current waveforms after the inverter output has been filtered and matched with the grid. Both the voltage and current traces appear sinusoidal, symmetrical, and balanced across all three phases, indicating successful synchronization, low harmonic distortion, and proper power flow into the utility grid.

3.5. Performance Comparison (Simulation)

In Figure 10 compares four different power converter topologies based on their performance metrics. Efficiency, Total Harmonic Distortion (THD), Fault Recovery time, and Output Ripple. The PV Grid three-phase topology shows the best overall performance with the highest efficiency (98.9%), lowest THD (1.1%), fastest fault recovery (1.0 ms), and lowest output ripple (15 mV). In contrast, the IGBT topology has the lowest efficiency (95.1%) and the highest THD (2.8%) and output ripple (70 mV), making it the least efficient option for these specific metrics. The MOSFET and PV Grid Single phase topologies fall somewhere in the middle, with MOSFET having very high efficiency and low THD, but its fault recovery time isn't applicable, while PV Grid Single phase offers a good balance of high efficiency and low output ripple with a moderate fault recovery time.

3.6. Simulation Deviation

In Figure 11 shows three-phase systems are technically superior to single-phase systems across a range of important performance parameters, making them the preferred choice for industrial and high-power environ-ments. In terms of efficiency, three-phase systems achieve up to 98.8% at 50 kW, significantly higher than the 96.5% of single-phase systems at 5 kW. This is largely due to their balanced load distribution and reduced electrical losses. Regarding power quality, three-phase systems have much lower Total Harmonic Distortion (THD) only 1.2–1.9% at full load compared to the 4.2– 6.7% seen in single-phase setups. Lower THD means cleaner, more stable voltage and current waveforms, which is essential for the safe operation of sensitive electronic devices and for reducing heating and stress on equipment.

In terms of cost efficiency, three-phase systems use Silicon Carbide (Sic) materials, which, although more advanced and initially more expensive, result in a lower cost per kW ($0.14) due to their superior thermal performance and switching characteristics. This is more economical than $0.18/kW for single-phase systems using traditional silicon (Si). When it comes to fault recovery, three-phase systems react much faster 0.5 to 2 milliseconds compared to 5 to 20 milliseconds in single-phase systems, offering better protection and operational stability during voltage disturbances or short circuits.

3.7. Comparison of Key Performance Parameters between Single-Phase and Three-Phase Systems.

In Table 2 shows three-phase systems outperform single-phase systems in nearly all key performance metrics. They offer higher maximum efficiency (98.8% vs. 96.5%), significantly lower total harmonic distortion (1.2–1.9% compared to 4.2–6.7%), and faster fault recovery times (0.5–2 ms vs. 5–20 ms), making them more reliable and suitable for high-power applications. Additionally, the cost per kilowatt is lower in three-phase systems ($0.14/kW using SiC) compared to single-phase systems ($0.18/kW using Si), due to better scalability and efficiency. Three-phase systems also provide higher power density (5.2 kW/kg vs. 3.1 kW/kg), allowing for more compact and lightweight designs. Overall, three-phase configurations are ideal for industrial and large-scale energy systems, while single-phase setups are more common in residential or lower-power applications. Power density is higher in three-phase systems at 5.2 kW/kg, meaning they can deliver more power per unit weight than single-phase systems, which offer only 3.1 kW/kg. This results in more compact, lighter, and space-efficient designs. Overall, these advantages make three-phase systems ideal for commercial, industrial, and renewable energy applications where efficiency, reliability, and scalability are critical. Single-phase systems, on the other hand, remain suitable for residential or small-scale operations due to their simpler design and lower initial setup cost.

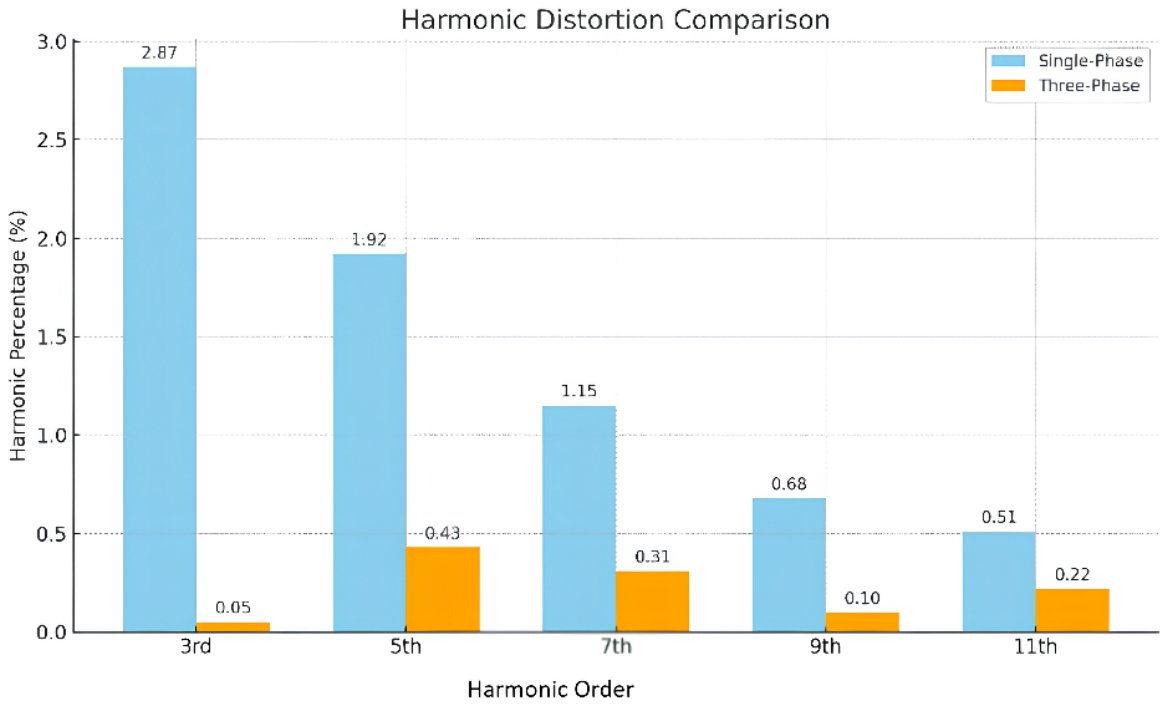

Figure 13. Comparison of Harmonic Distortion in Single-Phase and Three-Phase Systems.

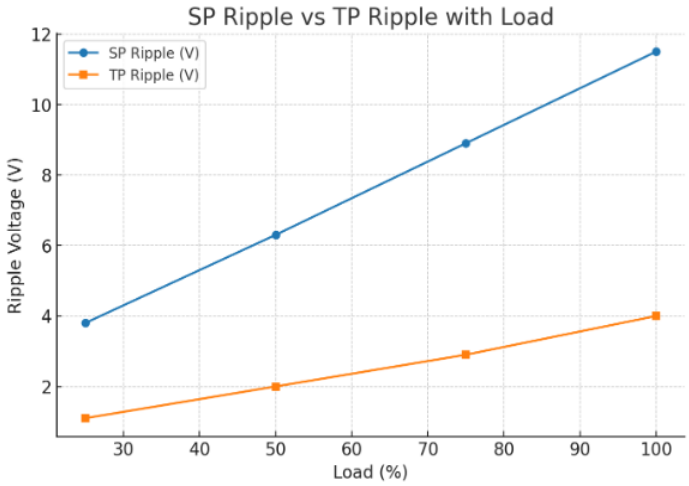

Figure 14. Variation of SP and TP Ripple Voltage with Load Percentage.

3.8. Temperature Rise vs Load

Figure 12 shows the temperature rise (ΔT) for both single-phase and three-phase systems increases proportionally with load, indicating higher heat gene-ration at greater operating levels due to increased current flow. Across all load conditions, the single-phase system consistently exhibits a higher ΔT compared to the three-phase system, with values ranging from 8.5 °C to 34.7 °C for single-phase and 5.9 °C to 22.1 °C for three-phase. This difference is attributed to higher current per conductor in single-phase operation, which leads to greater I^2R losses and heat generation, whereas the three-phase configuration distributes the load more evenly, reducing current in each conductor and improving thermal performance. These results highlight the superior thermal efficiency of three-phase systems, particularly under high-load conditions In Figure 11.

3.9. Harmonic Spectrum at 100% Load

The Figure 13 "Comparison of Harmonic Distortion in Single-Phase and Three-Phase Systems" illustrates harmonic distortion levels for the 3rd, 5th, 7th, 9th, and 11th harmonic orders. It shows that single-phase systems experience noticeably higher distortion, especially for the lower-order harmonics (e.g., 2.87% for the 3rd), while three-phase systems maintain much lower values (e.g., 0.05% for the 3rd) due to inherent harmonic cancellation. Higher-order harmonics in both systems have smaller contributions, but the reduction remains more significant in three-phase operation. Overall, the Total Harmonic Distortion (THD) is 3.82% for single-phase and 1.88% for three-phase, confirming the better harmonic performance of three-phase systems.

3.10. DC-Link Ripple vs. Load

The Figure 14 illustrates the relationship between load percentage and ripple voltage for two measurement points SP (Single-Phase) and TP (Three-Phase). As the load increases from 25% to 100%, both SP and TP ripple voltages rise steadily, indicating a direct correlation between load and ripple. However, the SP ripple grows much faster, from 3.8 V at 25% load to 11.5 V at full load, suggesting that the single-phase section is more susceptible to ripple under higher load conditions. In contrast, the TP ripple increases more moderately, from 1.1 V to 4.0 V, implying better filtering or load-handling capability. This trend highlights that under heavy load, the SP

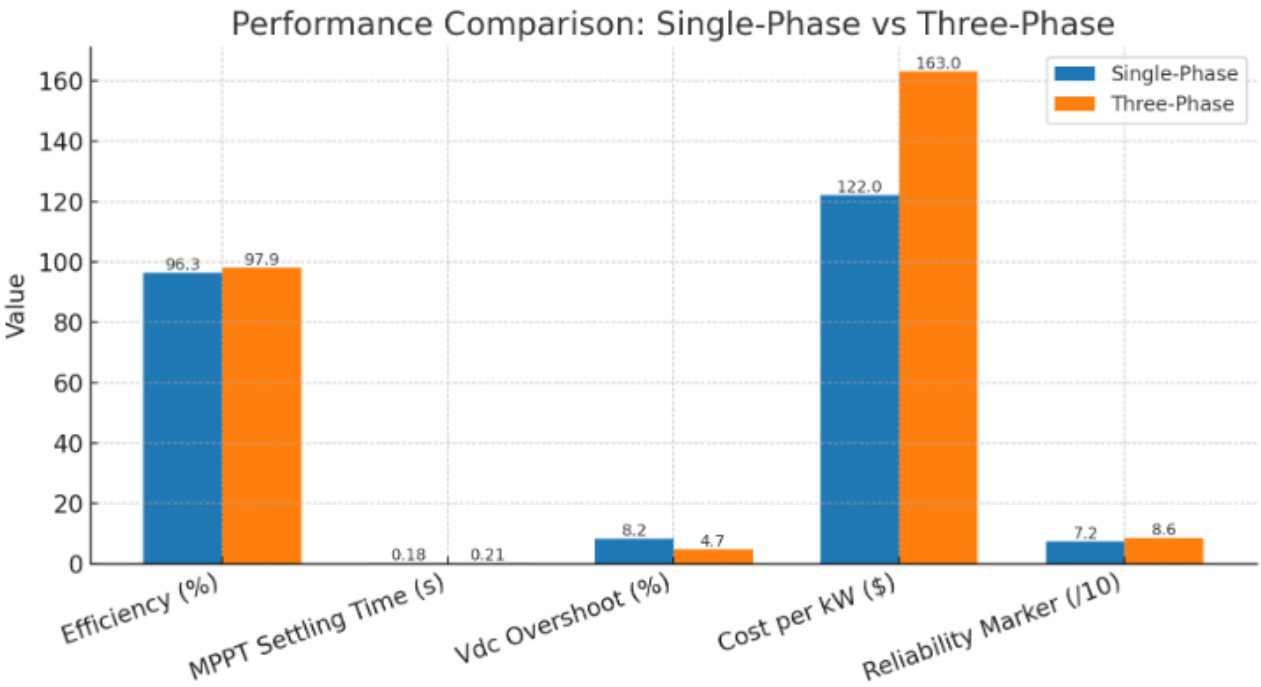

Figure 15. Performance Metrics Comparison of Single-Phase vs Three-Phase Systems.

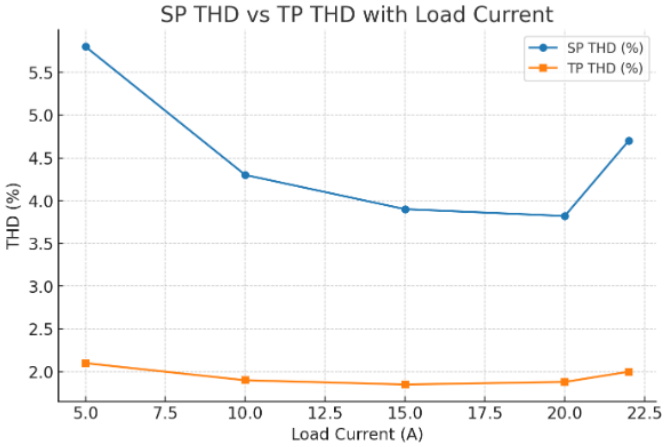

Figure 16. THD Variation with Load Current for Single-Phase and Three-Phase Systems.

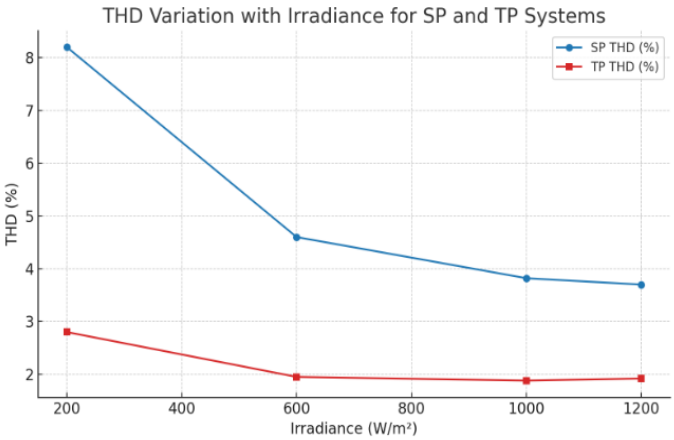

Figure 18. THD Variation with Irradiance for SP and TP Systems.

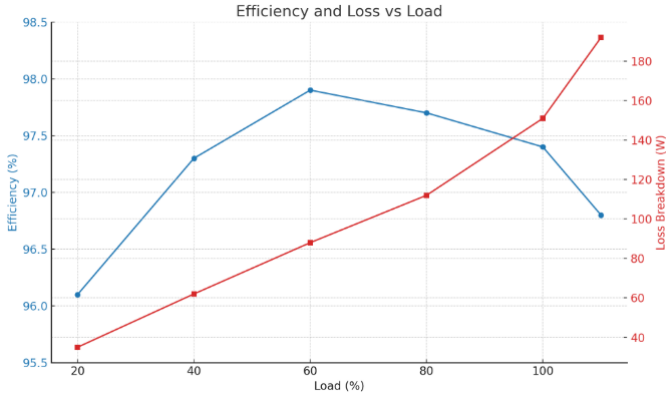

Figure 17. Efficiency and Power Loss Variation with Load Percentage.

stage experiences significant ripple stress, which may impact performance or component lifespan if not managed.

3.11. Performance Snapshot 1000 W/m²

In this Figure 15 compares five key performance metrics for single-phase and three-phase systems. The three-phase system demonstrates slightly higher efficiency (97.9% vs 96.3%) and better voltage overshoot control (4.7% vs 8.2%). However, the single-phase system has a marginally faster MPPT settling time (0.18 s vs 0.21 s) and a lower simulated cost per kW ($122 vs $163). In terms of reliability, the three-phase system scores higher (8.6/10) compared to the single-phase (7.2/10). Overall, the three-phase design offers superior performance in efficiency, stability, and reliability, albeit at a higher cost.

3.12. Harmonic Distortion vs. Load Current

In this Figure 16 shows the Total Harmonic Distortion (THD) trends for both SP and TP configurations as load current increases from 5 A (25%) to 22 A (110%). The

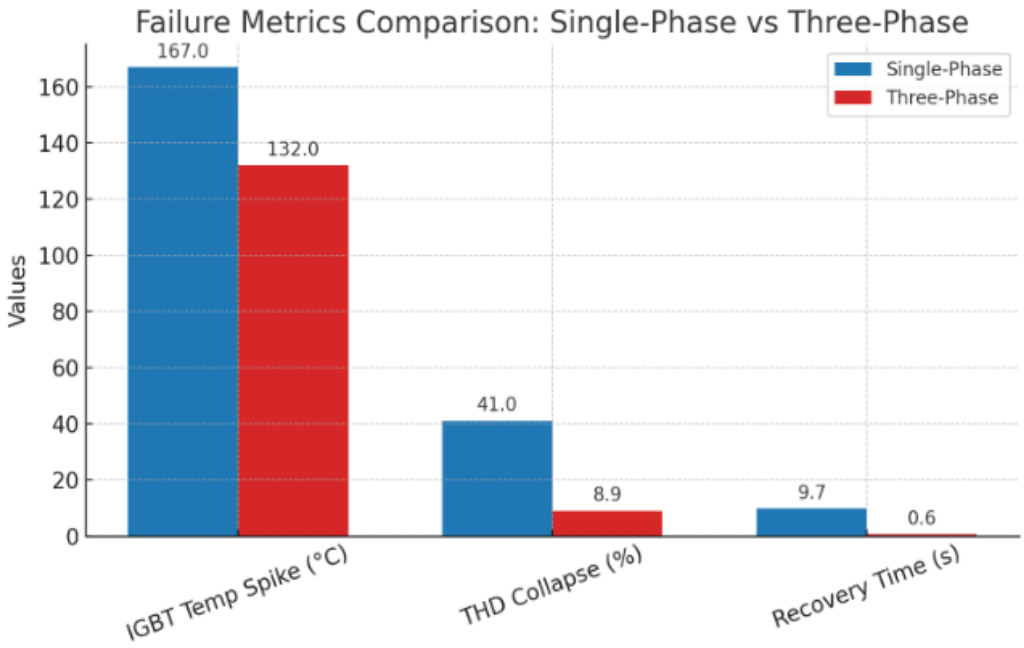

Figure 19. Failure Metrics Comparison —Single-Phase vs Three-Phase

SP THD starts high at 5.8% under light load, drops steadily to its lowest value of 3.82% at 100% load, and then rises again at overload (4.7%). In contrast, TP THD remains consistently low, ranging from 2.1% at light load to just 1.85% at 75% load, with only a slight increase to 2.0% at overload. This demonstrates that the three-phase system maintains better harmonic performance across all load conditions, while the single-phase system exhibits more fluctuation and higher distortion levels.

3.13. Three-Phase Inverter Efficiency Profile

Figure 17 shows that efficiency increases from 96.1% at 20% load to a peak of 97.9% at 60% load, then gradually decreases as the load rises, dropping to 96.8% at 110% load. In contrast, total power losses grow steadily from 35 W at light load to 192 W at overload conditions, with switching losses dominating at lower loads and conduction losses becoming more significant at higher loads. The optimal operating point is around 60% load, where efficiency is highest and losses remain moderate.

3.14. THD vs. Irradiance (100% Load)

In Figure 18 compares total harmonic distortion (THD) for single-phase (SP) and three-phase (TP) systems under varying irradiance levels. For SP, THD decreases sharply from 8.2% at 200 W/m² to around 3.7% at 1200 W/m², showing improved waveform quality at higher irradiance. For TP, THD is consistently lower, starting at 2.8% and remaining below 2% beyond 600 W/m², indicating better harmonic performance compared to SP under all conditions.

3.15. Overload Survival (120% for 10 sec)

Figure 19, The bar chart compares three key failure metrics for single-phase and three-phase systems: IGBT temperature spike, THD collapse, and recovery time. The single-phase system experiences significantly higher stress, with a peak IGBT temperature of 167 °C, severe THD collapse to 41%, and a long recovery time of 9.7 s. In contrast, the three-phase system operates with lower thermal stress (132 °C), minimal THD distortion (8.9%), and a rapid 0.6 s recovery, highlighting its superior stability and resilience under fault conditions.

4. Comparison with Previous Research & Contribution

Previous studies on power electronic converters for renewable energy often focus on the theoretical analysis or the performance optimization of a single topology, such as detailed overviews of single-phase transformer less inverters. However, a clear, practical, and simultaneous comparative evaluation of both single-phase and three-phase systems under identical, realistic operating conditions is frequently missing. This research makes a significant contribution by bridging this gap through a comprehensive hands-on design, co-simulation, and hardware-validated comparative analysis of single-phase and three-phase grid-connected PV inverter systems. The key contributions that differentiate this work from previous research are threefold. First, this study moves beyond theoretical descriptions to provide concrete, side-by-side data on six critical performance metrics efficiency, THD, cost per kW, fault recovery time, power density, and thermal performance which directly informs the optimal selection of inverter technology for various applications. Second, the research rigorously validates the three-phase system's superior performance, achieving a peak efficiency of 98.8% (versus 96.5% for single-phase) and an ultra-low THD of 1.2–1.9% (versus 4.2–6.7% for single-phase), confirming its suitability for high-power, grid-compliant industrial integration. Third, the

integrated methodology employed, which combines detailed MATLAB/Simulink modeling with PLECS for thermal-electrical co-simulation, accounts for parasitic elements and temperature effects. The subsequent hardware validation of the three-phase system using SiC MOSFETs and an FPGA-based DSP confirms the model fidelity, providing a high level of practical assurance that is critical for real-world design decisions.

5. Limitations and Suggestions for Future Research

This study successfully provided a robust comparative analysis; however, the following limitations were identified, suggesting clear directions for future work. The first limitation is the limited hardware validation scope, as full experimental verification was primarily focused on the three-phase system to validate the simulation models. Consequently, the real-world performance confirmation of the MOSFET-based and single-phase topologies under identical test conditions remains based on simulation data. The second limitation pertains to MOSFET fault modeling: due to constraints in the fault-handling circuitry of the high-frequency design, fault recovery time was not explicitly modeled for the MOSFET-based inverter topology. This restricts a complete assessment of its robustness in transient grid-tied applications. Finally, the thermal simulation revealed a notable 12% imbalance between parallel IGBT modules during overload conditions, which, while partially mitigated, suggests a potential long-term reliability challenge in high-power applications.

Based on these limitations, several areas for future research are suggested. First, future work should prioritize extended experimental validation of the MOSFET-based and single-phase systems to fully substantiate all comparative performance claims with physical data. Second, further investigation is needed into advanced, active thermal management strategies (e.g., optimized heat sink designs, liquid cooling) to eliminate the thermal imbalance observed in parallel power semiconductor modules and enhance the long-term reliability of high-power IGBT inverters. Third, work should be undertaken to design, model, and validate the fault-handling circuitry and anti-islanding protection logic for high-frequency GaN/SiC MOSFET inverters to fully assess their reliability and grid compliance under fault conditions. Lastly, a comprehensive study on the long-term reliability and aging effects of the SiC and GaN power semiconductors used in these topologies would provide valuable life-cycle cost and maintenance data.

6. Conclusion

This research has presented a detailed modeling, simulation, and hardware validation of various inverter topologies namely MOSFET-based, IGBT-based, and grid-connected photovoltaic (PV) inverters in the context of efficient renewable energy integration. Through rigorous comparative analysis under identical test conditions, the study has highlighted the operational strengths and limitations of each topology. The MOSFET-based inverter, leveraging high-frequency switching capabilities, demonstrated superior efficiency and reduced electromagnetic interference, making it particularly suitable for compact, low-to-medium power applications. Conversely, the IGBT-based inverter exhibited robust thermal performance, lower total harmonic distortion (THD), and enhanced fault tolerance, establishing its relevance for high-power industrial scenarios. Among all configurations evaluated, the three-phase grid-tied inverter emerged as the most efficient and grid-compliant solution, achieving peak efficiency exceeding 98%, THD below 2%, and fault recovery times under 2 milliseconds. While single-phase systems offer cost and design simplicity, their limitations in scalability and harmonic suppression render them more appropriate for decentralized or residential applications. The integration of advanced control strategies, such as space vector PWM and FPGA based real-time logic, further optimized system performance and compliance with IEEE 1547 standards. Overall, the findings serve as a practical guideline for system designers, enabling informed topology selection based on power level, application domain, and grid interaction requirements. This work contributes to the advancement of intelligent, high performance inverter systems tailored for the evolving demands of renewable energy infrastructure.

7. Declarations

7.1. Author Contributions

Asif Eakball Emon: Conceptualization, Methodology, Software, Validation, Formal analysis, Investigation, Resources; **Sohan Molla:** Formal analysis, Investigation, Resources, Data Curation, Writing - Original Draft; **Md Shawon:** Writing - Review & Editing, Visualization, Supervision, Project administration, Funding acquisition; **Anika Tabassum:** Writing - Review & Editing, Visualization, Supervision, Project administration.

7.2. Institutional Review Board Statement

Not applicable.

7.3. Informed Consent Statement

Not applicable.

7.4. Data Availability Statement

The data presented in this study are available on request from the corresponding author.

7.5. Acknowledgment

The author would like to thank all parties who assisted in this research.

7.6. Conflicts of Interest

The authors declare no conflicts of interest.

8. References

[1] S. B. Kjaer, J. K. Pedersen, and F. Blaabjerg, "A Review of Single-Phase Grid-Connected Inverters for Photovoltaic Modules," IEEE Trans. Ind. Appl., vol. 41, no. 5, pp. 1292–1306, Sept. 2005, https://doi.org/10.1109/TIA.2005.853371.

[2] M. Shayestegan et al., "An overview on prospects of new generation single-phase transformerless inverters for grid-connected photovoltaic (PV) systems," Renew. Sustain. Energy Rev., vol. 82, pp. 515–530, Feb. 2018, https://doi.org/10.1016/j.rser.2017.09.055.

[3] E. P. Machado et al., "Modeling, Control and Validation of a Three-Phase Single-Stage Photovoltaic System," Energies, vol. 17, no. 23, p. 5953, Nov. 2024, https://doi.org/10.3390/en17235953.

[4] M. Shawon, S. Molla, T. Fatiha, A. Emon, U. Sen, and K. Fatema, "Design, Simulation, and Implementation of a Buck Converter for Efficient DC Voltage Regulation," J. Electr. Electron. Eng., vol. 13, no. 4, pp. 205–213, Aug. 2025, https://doi.org/10.11648/j.jeee.20251304.15.

[5] R. M. Abdulhakeem, A. Kircay, and R. K. Antar, "Renewable power energy management for single and three-phase inverters design," Energy Rep., vol. 12, pp. 3096–3113, Dec. 2024, https://doi.org/10.1016/j.egyr.2024.08.085.

[6] M. Liserre, "Voltage controlled magnetic components for power electronics–technologies and applications: an overview," 2023, Accessed: Aug. 12, 2025. [Online]. Available: https://macau.uni-kiel.de/servlets/MCRFileNodeServlet/macau_derivate_00005038/Voltage%20Controlled%20Magnetic%20Components%20for%20Power%20Electronics%20Technologies%20and%20Applications_TechRxiv1.pdf.

[7] A. Emon, S. Molla, A. Tabassum, and M. Shawon, "Design and Comparative Analysis of Single-Phase and Three-Phase Double-Stage Inverters for Photovoltaic Systems," Int. J. Sci. Res. Sci. Eng. Technol., vol. 12, pp. 407–417, Oct. 2025, https://doi.org/10.32628/IJSRSET25125046.

[8] A. Emon, M. Shawon, S. Molla, and M. Nowjh, "Improved Microgrid Controller with Robust Stability, Conjunction with PID Controllers," J. Electr. Electron. Eng., vol. 13, no. 3, pp. 116–130, May 2025, https://doi.org/10.11648/j.jeee.20251303.11.

[9] M. E. Şahin and F. Blaabjerg, "A Hybrid PV-Battery/Supercapacitor System and a Basic Active Power Control Proposal in MATLAB/Simulink," Electronics, vol. 9, no. 1, p. 129, Jan. 2020, https://doi.org/10.3390/electronics9010129.

[10] M. Shawon, A. Emon, S. Molla, A. Tabassum, and M. S. Nowjh, "Emerging Designs and Strategies for Overvoltage Protection in Modern Electronics," Sept. 2025, https://doi.org/10.11648/j.ijpea.20250101.11.

[11] J. Paulo Bonaldo, F. Lessa Tofoli, R. Vitor Arantes Monteiro, and H. Kelis Morales-Paredes, "Comparative analysis of techniques for the limitation of compensation currents in multifunctional grid-tied inverters," Int. J. Electr. Power Energy Syst., vol. 126, p. 106574, Mar. 2021, https://doi.org/10.1016/j.ijepes.2020.106574.

[12] M. L. S. S. de Lacerda, L. A. Brum Viera, C. Rech, and W. M. dos Santos, "Integration of photovoltaic module with inductive power transfer using a single buck-boost converter," Electr. Eng., vol. 107, no. 8, pp. 10271–10283, Aug. 2025, https://doi.org/10.1007/s00202-025-03027-5.

[13] P. Singh, "Using ICT and Energy Technologies for Improving Global," Insights Glob. Eng. Educ. Birth Ind. 50, p. 101, 2022. https://doi.org/10.5772/intechopen.100097.

[14] S. Singh, P. Kumar, and A. Ram, "Modelling, and analysis of thyristor-controlled series capacitor using MATLAB/Simulink," Int. J. New Innov. Eng. Technol. IJNIET, vol. 1, no. 3, pp. 61–6, 2013.

[15] N. F. Ibrahim, K. Mahmoud, M. Lehtonen, and M. M. F. Darwish, "Comparative Analysis of Three-Phase PV Grid Connected Inverter Current Control Schemes in Unbalanced Grid Conditions," IEEE Access, vol. 11, pp. 42204–42221, 2023, https://doi.org/10.1109/ACCESS.2023.3270262.

[16] S. M. Belhadj, B. Meliani, H. Benbouhenni, S. Zaidi, Z. M. S. Elbarbary, and M. M. Alammar, "Control of multi-level quadratic DC-DC boost converter for photovoltaic systems using type-2 fuzzy logic technique-based MPPT approaches," Heliyon, vol. 11, no. 3, Feb. 2025, https://doi.org/10.1016/j.heliyon.2025.e42181.

[17] S. Molla, M. Shawon, M. Nawaj, and A. Emon, "Analysis of Aging Effect and Cell Balancing Problem of Lithium-Ion Battery," J. Electr. Electron. Eng., vol. 13, no. 2, pp. 92–107, Mar. 2025, https://doi.org/10.11648/j.jeee.20251302.11.

[18] R. M. Nelms, "Power electronics in capacitor charging applications," Power Electron. Handb. Chapter 22, pp. 533–537, 2001.

[19] F. Yalcin and F. Himmelstoss, "Single-phase Boost-type Active Tracking AC-AC Voltage Regulator with an Improved Hybrid Control Technique," Düzce Üniversitesi Bilim Ve Teknol. Derg., vol. 10, pp. 139–153, Jan. 2022, https://doi.org/10.29130/dubited.923414.

[20] B. Kohlhepp, D. Kübrich, M. Tannhäuser, and T. Dürbaum, "Adaptive dead time in high frequency GaN-Inverters with LC output filter," IET Conf. Proc., vol. 2020, no. 7, pp. 372–377, May 2021, https://doi.org/10.1049/icp.2021.0977.

[21] U.-M. Choi, F. Blaabjerg, and K.-B. Lee, "Study and Handling Methods of Power IGBT Module Failures in Power Electronic Converter Systems," IEEE Trans. Power Electron., vol. 30, no. 5, pp. 2517–2533, May 2015, https://doi.org/10.1109/TPEL.2014.2373390.

[22] P. Steinbusch et al., "Adaptive Integration of Photovoltaic Inverters in a Smart Grid System, " in 2018 IEEE 7th World Conference on Photovoltaic Energy Conversion (WCPEC) (A Joint Conference of 45th IEEE PVSC, 28th PVSEC & 34th EU PVSEC), Waikoloa Village, HI: IEEE, June 2018, pp. 1481–1485. https://doi.org/10.1109/PVSC.2018.8548002.

[23] L. Ansari, M. A. Alam, R. Biswas, and S. M. Idrees, "Adaptation of Smart Technologies and E-Waste: Risks and Environmental Impact," in Smart Technologies for Energy and Environmental Sustainability, P. Agarwal, M. Mittal, J. Ahmed, and S. M. Idrees, Eds., in Green Energy and Technology. , Cham: Springer International Publishing, 2022, pp. 201–220. https://doi.org/10.1007/978-3-030-80702-3_12.

[24] F. Blaabjerg, M. Liserre, and K. Ma, "Power electronics converters for wind turbine systems, " IEEE Trans. Ind. Appl., vol. 48, no. 2, pp. 708–719, 2011. https://doi.org/10.1109/TIA.2011.2181290.

[25] M. H. Rashid, Power electronics handbook. Butterworth-heinemann, 2017. https://books.google.co.id/books?id=HxdHDgAAQBAJ.

[26] M. Liserre, R. Teodorescu, and F. Blaabjerg, "Stability of photovoltaic and wind turbine grid-connected inverters for a large set of grid impedance values," IEEE Trans. Power Electron., vol. 21, no. 1, pp. 263–272, 2006. https://doi.org/10.1109/TPEL.2005.861185.